

# Looking for quark saturation in proton and nuclei

Wei Zhu<sup>a</sup>, Rong Wang<sup>b</sup> and Jianhong Ruan<sup>a</sup>

<sup>a</sup>Department of Physics, East China Normal University, Shanghai 200062, P.R. China

<sup>b</sup>Institute of Modern Physics, Chinese Academy of Sciences, Lanzhou 730000, P.R. China

## Abstract

The quark saturation behavior at low  $Q^2$  is shown in numeric solution of the DGLAP equation with parton recombination corrections, which resembles the widely discussed JIMWLK saturation of gluons. Our calculation suggests that the partonic saturation can be interpreted as a dynamical balance between the splitting and the fusion processes of partons, without any condensation mechanisms added. The nuclear shadowing saturation at small  $x$  resulted from the proposed quark saturation is also discussed.

PACS number(s):

*keywords:* Quark saturation; Nuclear shadowing saturation

# 1 Introduction

The Jalilian-Marian-Iancu-McLerran-Weigert-Leonidov-Kovner (JIMWLK) equation [1] sums the contributions of multi-gluon fusions to the Balitsky-Fadin-Kuraev-Lipatov (BFKL) evolution [2]. An interesting property of this equation is a flattish solution of the unintegrated gluon distribution  $\phi_g(x, k_T)$  in the region of small transverse momentum  $k_T < Q_s$ , in which  $Q_s$  is commonly referred as the saturation scale. Assuming that the transition into the saturation region occurs abruptly near  $k_T \sim Q_s$ , one can find that the major gluons in this saturation solution have transverse momentum  $k_T \sim Q_s$ . This special solution is speculated as a new state of matter - the color glass condensation (CGC), which has been discussed a lot. However, the nature of the CGC is still unclear.

Generally, the partonic saturation implies that the occupation of partons in a fast proton reaches a limit and stop growing up. To estimate the saturation scale simply, one can apply the following naive picture [3]. The integrated parton distributions  $xf(x, Q^2)$  at scale of  $Q^2$  is the number of partons per unit rapidity interval. Therefore the transverse area per parton is  $\pi R_N^2/xf(x, Q^2)$  in a nucleon of radius  $R_N$ , and the cross section for two parton interaction can be estimated to be as  $C\alpha_s/Q^2$ , in which  $C$  is a model-dependent factor. The saturation effect is important when the number of partons per unit of rapidity times the gluon-gluon interaction cross section approaches the geometric size of the nucleon. We call it a full occupation. Under this assumption, the corresponding scale  $Q_s$  can be estimated by

$$Q_s^2 = C\alpha_s \frac{xf(x, Q_s^2)}{\pi R_N^2}. \quad (1)$$

The saturation critical boundary  $Q_s(x)$  separates the dilute and dense parton systems in the  $(x, Q^2)$  plane. Assuming  $xf(x, Q^2) = \pi R_N^2 Q^2/(C\alpha_s)$  is hold at  $Q < Q_s$ , this flat dis-

tribution is a clear feature of the saturation. Note that it is difficult to determine the value of  $Q_s$  in the experiment because the transition into saturation may do not occur abruptly, even though  $Q_s$  can be given in a more detailed calculation. From above estimation, the following saturation features are found, which is useful in searching/discriminating the partonic saturation in experiments. (i) The distribution is strong  $Q^2$ -dependent as  $xf(x, Q^2) \sim \alpha_s^{-1}Q^2$  at  $Q < Q_s$ , while it is weak  $Q^2$ -dependent as  $xf(x, Q^2) \sim \ln(Q/\Lambda_{QCD})$  at  $Q \gg Q_s$  according to the standard linear QCD evolution equations; (ii) The values of  $xf(x, Q^2)$  at  $Q < Q_s$  are  $x$ -independent if  $x$  is small enough; (iii) The corresponding unintegrated parton distribution  $\phi(x, k_T^2) \simeq \partial xf(x, Q^2)/\partial Q^2|_{Q^2=k_T^2}$  in the  $k_T\phi(x, k_T) \sim k_T$  has a peak at  $k_T \sim Q_s$ .

The deep inelastic scattering (DIS) data at small  $x$  and low  $Q^2$  is an interesting domain, where the partons have a larger correlation length  $\sim 1/Q$  and stronger recombination strength. It should especially be paid attention for studying the saturation physics. In this paper, we try to look for the possible quark saturation at low  $Q^2$ . In our previous work [4] the parton distributions in the proton are dynamically generated from a extreme low resolution scale where the nucleon have merely valence quarks by using a nonlinear QCD evolution equation - the DGLAP equation with the recombination corrections [5]. We find that the produced sea quark distributions present a positive and flat distribution in the region of small  $x$  and low  $Q^2$ . It is surprised to find that the saturation behaviors are exhibited for the quark distributions, which will be detailed in Sec. 2.

At low  $Q^2$  scale, the parton distributions partly contribute to measured structure functions. The nonperturbative QCD contributions are not negligible to the structure functions, which makes it harder to look at the possible quark saturation signature at

low  $Q^2$ . In order to identify the quark saturation from the experimental data, we need to remove the nonperturbative contributions to the structure function  $F_2^p(x, Q^2)$  at  $Q^2 < 1\text{GeV}^2$ . The popular phenomenological model - the vector meson dominance (VMD) model [6] is used to mimic these nonperturbative corrections, which is described in Sec. 3.

In order to confirm the suggested quark saturation above, we investigate the previous experimental data of nuclear shadowing effect at small  $x$  and low  $Q^2$ . The nuclear shadowing saturation resulted from the quark saturation in nuclei, which shows a flat distribution at small  $x$  and low  $Q^2$ , is discussed in Sec. 4. Moreover, it is found that the nuclear shadowing effect has different  $Q^2$ -dependent behaviors inside and outside of the saturation domain. More precise experiments at low  $Q^2$  are needed to verify the quark saturation. Discussions and summary are given in Sec. 5.

## 2 A solution of the quark saturation in the nonlinear QCD evolution equation

The physics of parton distributions at low  $Q^2$  are rarely discussed. However it is interesting and important for it is related to the origins of sea quarks and gluons at high  $Q^2$ . In our previous work, the gluon and sea quark distributions in the proton at  $Q^2 < 1\text{GeV}$  given by the nonlinear evolution equation [5] are shown in Fig. 1. Fig. 1(c) presents one interesting saturation feature of sea quarks. The sea quark distribution  $xf_{sea}(x, Q^2)$  reach a plateau at  $x < 0.01$  and  $0.1\text{GeV}^2 < Q^2 < 0.6\text{GeV}^2$ , and the height of the plateau linearly goes up with  $Q^2$  increasing.

Two asymptotic curves  $xf_{sea}(x, Q^2) \propto \alpha_s^{-1}Q^2$  and  $xf_{sea}(x, Q^2) \propto \ln Q^2$  are shown together with our predicted sea quark distribution as a function of  $Q^2$  in Fig. 2, to demonstrate the different  $Q^2$  dependence at low and high  $Q^2$ . Sea quark distributions  $xf_{sea}(x, Q^2)$  generated by the DGLAP [7] evolution are also shown. The obvious difference between distributions by nonlinear evolution and the DGLAP evolution indicates that the nonlinear effect is big in low  $Q^2$  range. It is easy to find the saturation features (i) and (ii) discussed in Sec. 1 in our predicted quark distributions. The coincidence of the predicted parton distributions at different  $x$  in Fig. 2b implies a geometrical scaling behavior  $xf_{sea}(x, Q^2) = \psi(Q^2/\Lambda_{QCD}^2)$ .

A more clear evidence of the quark saturation solution is presented in Fig. 3, which is the unintegrated quark distribution  $\phi_{sea}(x, k_T^2) \simeq [\partial xf_{sea}(x, Q^2)/\partial Q^2]|_{Q^2=k_T^2}$ , where the contributions of the Sudakov factor are neglected at very small  $x$  [8]. Note that our resulting curves are extracted from the data, which contain the experimental errors. A smaller uncertainty in  $f_{sea}(x, Q^2)$  calculation results in some obvious undulation in

$\phi_{sea}(x, k_T^2)$ . Hence in the geometrical scaling range, the parton distributions at different  $x$  are not ideally coincident (Fig. 2b). In Fig. 3, the unintegrated quark distributions in the saturation domain vary in a narrow range (the shadowed region in Fig. 3), instead of a plateau line predicted by the JIMWL equation.

Our predicted unintegrated quark distribution  $k_T\phi_{sea}(x, k_T^2)$  (multiplied by the phase space factor of the quark transverse momentum  $k_T$ ) as a function of  $k_T$  is shown in Fig.4, which demonstrates that the major sea quarks accumulated near  $k_T \sim Q_s$ . We call the peak of the largest occupation numbers the quark saturation rather than the condensation. One can find the quark distributions transit from the normal diluted parton state to a saturation limit though a broad domain, i.e., the transition into the saturation does not occur abruptly. For comparison, similar distributions but for the gluon density in the GBW (Golec-Biernat Wüsthoff) model [9] are shown in Fig. 5. This model is generally used to simulate the JIMWLK gluon saturation. Note that the GBW gluon lacks  $1/k_T$  tail because the parton evolution is not treated in this model.

One surprise is that there is no obvious saturation features of gluon distribution in the low  $Q^2$  range (See Fig. 1(a)), although the shadowing effect for gluon distribution is much stronger than that for sea quark distributions as the two leading nonlinear corrections are both from  $P_{gg \rightarrow gg} \sim 1/x$  and  $P_{q\bar{q} \rightarrow gg} \sim 1/x$  at small  $x$  [5]. This fact can be understood as follows. New radiated gluons from the fast valence quarks continually join the gluon evolution in the starting evolution scale, and they break the possible saturation balance for the gluon splitting and combing. This situation is different from the JIMWLK saturation for the gluon distribution, where the gluon splitting dominates the radiation of valence quarks at small  $x$ , because  $Q_s > 1\text{GeV} \gg \mu$  is far from the evolution starting scale. The

gluons directly radiated from the valence quarks is relatively less at high  $Q^2$  scale.

The phenomenon of the gluon saturation widely discussed is known as the CGC. Current theoretical understanding suggests that the CGC is the collective gluon excitations due to the JIMWIK equation sums all orders of gluon fusions. However, the quark saturation from nonlinear evolution equation has the similar CGC features, which suggests that the partonic (gluon and quark) saturation is a dynamical balance between strong splitting and fusion processes rather than a new condensation matter state. The origin of partonic (gluon and quark) saturation does not need any condensation dynamics.

### 3 Quark saturation in the proton structure function at low $Q^2$

Is the quark saturation only a mathematic solution in a nonlinear QCD evolution equation, or a real physical fact? To answer this question, we should look for the observable signs of the quark saturation in experiments. Parton distribution functions are extracted from the measured structure functions, however the nonperturbative QCD contributions are mixed with the possible saturation signature at low  $Q^2$ . In fact, at low  $Q^2$ , the multi-parton correlations dominate, and the inclusive lepton-nucleon cross section is mainly from the complicate higher twist interactions. According to the operator product expansion (OPE), the proton structure function  $F_2^p(x, Q^2)$  can be written as a series in  $1/Q^2$ ,

$$F_2^p(x, Q^2) = F_2^{LT}(x, Q^2) + F_2^{HT}(x, Q^2). \quad (2)$$

The leading (twist-2) term corresponds to scattering from one single free parton, while higher twist terms correspond to multi-parton interactions. Up to date, only a part of higher twist effects, for example, the recombination of initial partons (Fig. 6b) has been calculated perturbatively in terms of the corrections to the evolution equation of the parton distributions, which have been discussed in the previous section. We denote this parton contribution to the structure function as  $F_2^{DGLAP+ZRS}(x, Q^2)$ . However, we can neither perform nor interpret a partonic calculation of higher twist effects of the correlations between the initial and finite partons, since they break the factorization schema. In a certain kinematic regime, some of such higher twist contributions to  $F_2^p(x, Q^2)$  appear to be some observable hadronic phenomena. For this case, we may chose a suitable phenomenological model to describe the corresponding higher twist effects.



We try to use the well known Vector Meson Dominance (VMD) model to mimic the mentioned higher twist corrections above. The contributions shown in Fig. 6(c) can not be neglected at low  $Q^2$  due to the corrections of quark-antiquark pair, which interacts with the target like a virtual vector meson if the transverse momentum  $k_{\perp} \sim Q$  of quark pair is not large, and confinement effects are essential. Since contribution shown in Fig. 6(c) can not be factorized, we apply a phenomenological VMD model (Fig. 7) to describe it. Traditionally, the VMD model was used to explain the structure function at low  $Q^2$  region [10]. We denote this contribution as  $F_2^{VMD}(x, Q^2)$ .

In the VMD model,

$$F_2^{VMD}(x, Q^2) = \frac{Q^2}{4\pi\gamma_{\rho}^2} \frac{m_{\rho}^4 \sigma_{\rho p}}{(Q^2 + m_{\rho}^2)^2}. \quad (3)$$

where  $\gamma_{\rho}$  is the coupling constant between  $\rho$  vector meson and proton,  $x$  is a variable defined as  $x = Q^2/(s + Q^2 - m_p^2)$  rather than a momentum fraction of parton, and  $s$  is the CMS energy (W) square of the  $\gamma p$  collision. We consider the contributions of  $\rho$  meson only, since it is the dominant virtual particle involved. The cross sections  $\sigma_{\rho p}(W)$  is the total cross section of the virtual  $\rho$  meson scattering on the nucleon.

At high energy, the Regge theory [11] is successful to parameterize the cross sections  $\sigma_{\rho p}$ . The high energy behavior in Regge theory for the total cross section is expressed as  $\sigma_{\rho p}(s) \sim s^{\alpha_P - 1}$ , where  $\alpha_P = 1.0808$  is the intercepts of the Pomeron [12]. At large  $1/x$ , there is  $\sigma_{\rho p}(x) \sim x^{1 - \alpha_P}$ . The elastic scattering dominates in large  $x$  region for  $F_2^p(x, Q^2)$ . We neglect its contribution at large  $x$  in this work. In consequence,

$$F_2^{VMD}(x, Q^2) \simeq B \frac{m_{\rho}^2 Q^2}{(Q^2 + m_{\rho}^2)^2} x^{1 - \alpha_P} (1 - x)^{20}, \quad (4)$$

where  $B$  is a free parameter and determined to be  $B = 0.4$  from a fit to the experimental

data at low  $Q^2$ . An arbitrary large power in the factor  $(1-x)^{20}$  is applied to suppress the contributions of Pomeron at large  $x$ . Note that  $F_2^{DGLAP+ZRS}(x, Q^2)$  is taken from Ref. [4], which is fixed and determined by the experimental measurements at high  $Q^2 > 4 \text{ GeV}^2$ .

More complicated corrections to  $F_2^p(x, Q^2)$  at low  $Q^2$  are from the higher order QCD effects  $\mathcal{O}(\alpha_f)$  and the higher order recombination. In principle, we need to consider all these corrections, however it still worthwhile to look at the leading corrections first. Our interest is that if higher order corrections are small down to some low scale  $Q^2(\sim \mu^2)$ , then our leading order analysis of structure function data to  $\mu^2$  is acceptable. Otherwise, our calculation is still useful to extract the higher order contributions.

Finally, the proton structure function without higher order QCD effects and higher order recombinations is written as

$$F_2^p(x, Q^2) \simeq P F_2^{DGLAP+ZRS}(x, Q^2) + F_2^{VMD}(x, Q^2), \quad (5)$$

where  $P$  is the probability of inelastic events via bare photon-parton interaction. As  $m_\rho^4/(Q^2 + m_\rho^2)^2$  in Eq. (4) is the probability of the VMD event,  $P$  in Eq. (5) for the single parton scattering is then given by

$$P = 1 - \frac{m_\rho^4}{(Q^2 + m_\rho^2)^2}. \quad (6)$$

The results of our model is compared to experimental measurements [12-15] in Fig. 8 (at  $Q^2 < 1\text{GeV}^2$ ) and in Fig. 9 (at  $Q^2 > 1\text{GeV}^2$ ). The qualities of the fits are good. Our model in terms of the quark saturation gives results which is consistent with the observable data.

## 4 Quark saturation in the nuclear structure functions at low $Q^2$

The cross section ratios of inelastic muon scattering on nuclei to that on deuterium at very small  $x$  ( $0.00002 < x < 0.25$ ) and low  $Q^2$  down to  $0.03 GeV^2$  was measured by Fermilab experiment E665 [16]. The cross section ratio shows a platform at  $x < 10^{-3}$ . This nuclear shadowing platform was confirmed by the later NMC data [17]. These flat distributions are sign of the quark saturation.

The saturation found in the structure function ratio is related to two different saturation mechanisms. The saturation in  $F_2^{DGLAP+ZRS}(x, Q^2)$  resulted from the quark saturation has been discussed in Sec. 2. The quark saturation also exists in the nuclear quark distributions as shown in Fig. 1(d). The other mechanism for the saturation of nuclear structure function ratio is the hadron part of the structure function  $F_2^{VMD}$  which originated from the multiple-scattering of virtual meson off nuclei. In the VMD model for the nuclei,

$$F_2^{A,VMD}(x, Q^2) = \frac{Q^2}{4\pi\gamma_\rho} \frac{m_\rho^4 \sigma_{\rho A}}{(Q^2 + m_\rho^2)^2}. \quad (7)$$

Using the Glauber eikonal approximation [18], the relation between the total cross sections  $\sigma_{VA}$  and  $\sigma_{VN}$  is given by

$$\sigma_{\rho A} = 2 \int d^2b [1 - e^{-\sigma_{\rho p} T_A(b)/2}] \simeq G(R_A/l_V) \sigma_{Vp}, \quad (8)$$

where  $T_A(b)$  is the nuclear thickness function and

$$G(x) = \frac{3}{x^3} \left[ (1+x)e^{-x} - 1 + \frac{1}{2}x^2 \right], \quad (9)$$

$l_v$  is the mean free path of the hadronic fluctuation constituent of the virtual photon [19].

It is expected that  $l_V$  is much larger than the mean free path of the real vector meson

in the nucleus. Figure 10 shows the results of nuclear structure function ratios at low  $Q^2$  using  $l_V = 8$  fm. There is strong kinematic correlation between  $x$  and  $Q^2$  in the fixed target experiments, which makes low  $x$  measurements also with low  $Q^2$ . Our predicted ratios at  $x < 10^{-3}$  exhibit a weak dependence on  $x$  and  $Q^2$ , which are consistent with the experimental data. However more precise measurements are highly needed. A wide range of energy and of four-momentum transfer of the future Electron-Ion Collider (EIC) would provide valuable opportunities to search the quark saturation.

The other possible solution for the structure function ratio saturation is also considered: the shapes of quark distribution functions in proton and nucleus are similar towards small  $x$  at large  $Q^2$ . Our predicted  $F_2^p(x, Q^2)$  and  $F_2^{Ca}(x, Q^2)$  at  $Q^2 \gg 1\text{GeV}^2$  are shown in Fig. 11, where the nonlinear corrections are negligible. The  $Q^2$ - and  $x$ -dependent behaviors of the nuclear shadowing are different from the nuclear shadowing saturation in Fig. 12.

## 5 Discussions and Summary

The typical parton evolution configuration of the proton in  $(x, Q^2)$  space is shown in Fig. 13. The starting point is the proton at low  $\mu^2$ , which is represented as three valence quarks. With the increase of the virtuality of the probe while the value of  $x$  is fixed, we are able to resolve the partons into smaller ones. This type of evolution is well described by the DGLAP equation at large  $x$ , and the DGLAP equation including parton recombination corrections at small  $x$ . In the first case, the number of partons rises logarithmically while their typical size decreases like  $\alpha_s/Q^2$  so that the partons in the proton become more and more dilute. However in the second case, the number of sea quarks rises as  $\sim Q^2/\alpha_s$ , and it keeps on the full occupation (splitting and fusion balance), which leads to the quark saturation. In a little larger  $Q^2$  but very small  $x$  range, BFKL evolution with gluon recombination, namely the BK evolution (with leading recombination) and JIMWLK evolution (with multi-recombinations) towards smaller  $x$  with  $Q^2$  fixed are commonly used. The proton in the JIMWLK evolution tends to be the black-disc limit for which the gluons are fully overlapped, namely, the JIMWLK saturation. The quark saturation originates from the leading order parton recombinations with big strong coupling constant in low  $Q^2$ . The saturation for the quark distributions can not be directly probed in the deep inelastic scattering at low  $Q^2$ , since the hadronic component of the probe is mixed with the quark saturation. The gluon saturation by the JIMWLK equation is the result of multi-recombination with small strong coupling constant, which is also can not be observed directly by the electro-magnetic probe. It is very interesting that these two kinds of saturation have the similar features, which suggests that both the quark saturation and gluon saturation comes from the dynamic balance between the parton recombination and

parton splitting.

In summary, a numeric solution of the DGLAP equation with parton recombination corrections at low  $Q^2$  shows the quark saturation, which likes the JIMWLK saturation of gluons. This calculation shows that the partonic saturation is the result of the dynamical balance between parton splitting and fusion in perturbative QCD theory. The observed nuclear shadowing saturation interpreted as the quark saturation is discussed. We argue that the nuclear shadowing saturation measured by E665 and NMC collaborations is the possible sign of the quark saturation.

## References

- [1] J. Jalilian-Marian, A. Kovner, L. McLerran, and H. Weigert, Phys. Rev. **D55** 5414 (1997); J. Jalilian-Marian, A. Kovner, A. Leonidov, and H. Weigert, Nucl. Phys. **B504**, 415 (1997); H. Weigert, Nucl. Phys. **A703**, 823 (2002); E. Iancu, A. Leonidiv, and L. McLerran, *ibid.* **A692**, 583 (2001); Phys. Lett. **B510**, 133 (2001).
- [2] L.N. Lipatov, Sov. J. Nucl. Phys. **23**, 338 (1976); V.S. Fadin, E.A. Kuraev, L.N. Lipatov, Phys. Lett. **B60**, 50 (1975); E.A. Kuraev, L.N. Lipatov, V.S. Fadin, Sov. Phys. JETP **44**, 443 (1976); E.A. Kuraev, L.N. Lipatov, V.S. Fadin, Sov. Phys. JETP **45**, 199 (1977); I.I. Balitsky, L.N. Lipatov, Sov. J. Nucl. Phys. **28**, 822 (1978); I.I. Balitsky, L.N. Lipatov, JETP Lett. **30**, 355 (1979).
- [3] L.V. Gribov, E.M. Levin and M.G. Ryskin, Phys. Rep. **100**, 1 (1983).
- [4] X.R. Chen, J.H. Ruan, R. Wang, P.M. Zhang and W. Zhu, Int. J. Mod. Phys. **E23**, 14500058 (2014), hep-ph/1306.1872.
- [5] W. Zhu, Nucl. Phys. **B551**, 245 (1999) [arXiv:hep-ph/9809391]; W. Zhu, J.H. Ruan, Nucl. Phys. **B559**, 378 (1999) [arXiv:hep-ph/9907330v2]; W. Zhu and Z.Q. Shen, HEP & NP, **29**, 109 (2005)[arXiv:hep-ph/0406213v3].
- [6] J.J. Sakurai, currents and mesons, university of Chigag, Chigago (1969); T. H. Bauer et al., Rev. Mod. Phys. **50**, 261 (1978); G. Grammer and J. D. Sullivan, in Electromagnetic Interactions of Hadrons, edited by A. Donnachie and G. Shaw, Plenum, New York, 1978, Vol.2.

- [7] G. Altarelli and G. Parisi, Nucl. Phys. **B126**, 298 (1977); V.N. Gribov and L.N. Lipatov, Sov. J. Nucl. Phys. **15**, 438 (1972); Yu.L. Dokshitzer, Sov. Phys. JETP. **46**, 641 (1977).
- [8] M.A. Kimber, A.D. Martin and M.G. Ryskin, Phys. Rev. **D63**, 114027 (2001).
- [9] K. J. Golec-Biernat and M. Wüsthoff, Phys. Rev. **D59**,014017 (1998); Phys. Rev. **D60**, 114023 (1999).
- [10] B. Badelek, J. Kwieciski, B. Ziaja, Eur. Phys. J. **C26**, 45 (2002); Acta Phys. Polon. **B33**, 3701 (2002).
- [11] P.D.B. Collins, An Introduction to Regge Theory and High Energy Physics, Cambridge University Press, Cambridge, 1977.
- [12] A. Donnachie and P. V. Landshoff, Physics Letters **B437**, 408 (1998).
- [13] ZEUS Collab., J. Breitweg, et al., Phys. Lett. **B487** 53 (2000).
- [14] NMC Collab., M. Arneodo, et al., Nucl. Phys. **B483**, 3 (1997); E665 Collab., R. Adams et al., Phys. Rev. **D54**, 3006 (1996); H1 Collab., S. Aid, et al., Nucl. Phys. **B470**, 3 (1996); H1 Collab., C. Adloff et al., Nucl. Phys. **B497**, 3 (1997); Eur. Phys. J. **C21**, 33 (2001). ZEUS Collab., J. Breitweg et al., Phys. Lett. **B407**, 432 (1997); M. Derrick et al., Z. Phys. **C69**, 607 (1996); M. Derrick et al., Z. Phys. **C72**, 399 (1996).
- [15] JLab., V. Tvaskis et. al., Phys.Rev. **C81**, 055207 (2010).
- [16] E665 Collab., M.R.Adams, et. al., Phys. Rev. Lett. **68**, 3266 (1992); Z.Phys. **C67**, 403 (1995).



- [17] NMC Collab., Arneodo et al., Nucl. Phys. **B441**, 12 (1995); Amaudruz et al., Zeit. Phys. **C51**, 387 (1991).
- [18] R.J. Glauber, in Lectures in theoretical physics, ed. W.E. Brittin et al. (Interscience Publishers, New York, 1959); R.J. Glauber and G. Matthiae, Nucl. Phys. B 21, 135 (1970).
- [19] G.Grammar and J.D.Sullivan, in: Electromagnetic Interactions of Hadrons (Vol.2), eds. A.Donnachie and G.Shaw (Plenum Press, New York, 1978).

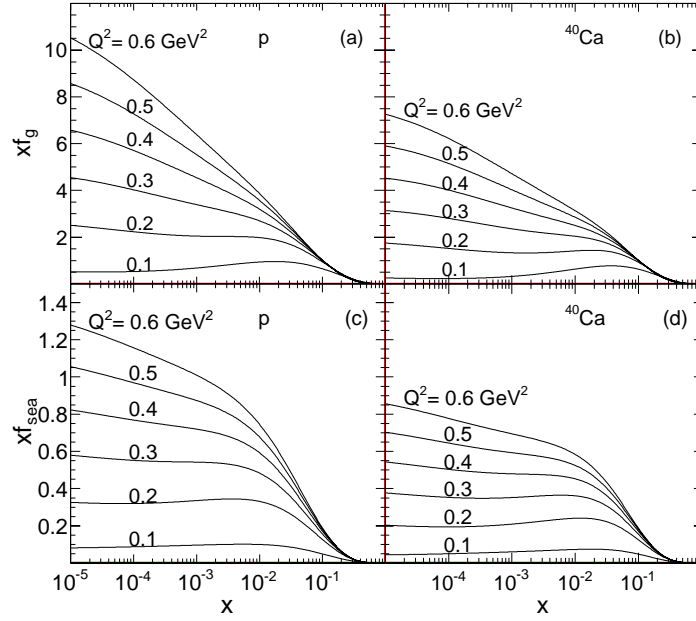


Figure 1: Our predicted parton distributions at the low  $Q^2$  range, where the platform is appeared in the quark distributions.

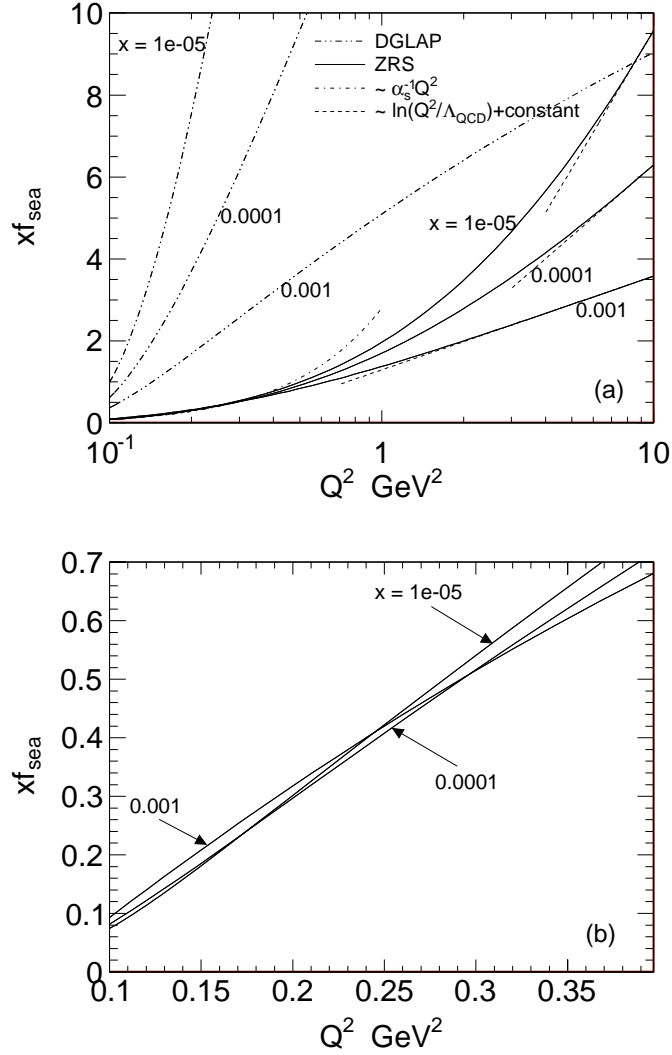


Figure 2: Our predicted proton structure functions (solid curves) at low  $Q^2$  and small  $x$ . The dashed lines are asymptotic lines: (left)  $xf_{sea} \sim \alpha_s^{-1}Q^2$  and (right)  $xf_{sea} \sim \ln Q^2$ . The broken curves are the solutions of the linear DGLAP equation. The translation of two asymptotic behaviors and the distributions coincide are the characters of the parton saturation.

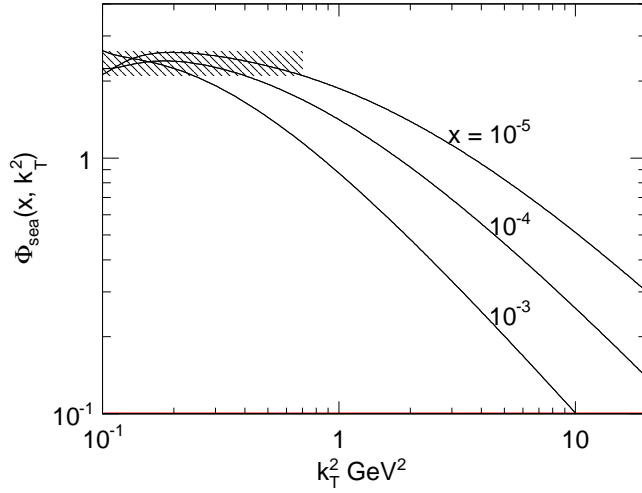


Figure 3: Unintegrated sea quark distributions in the proton at low  $Q^2$ . The cloud range presents quark saturation.

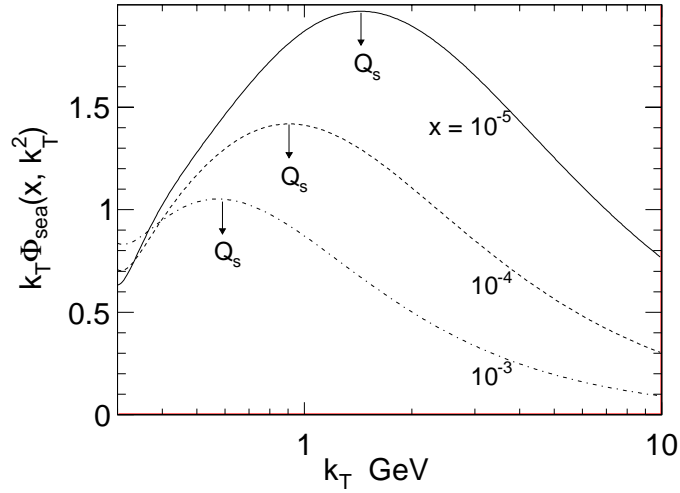


Figure 4: Unintegrated sea quark distributions in the proton (multiplied by the phase space factor of the quark transverse momentum  $k_T$ ) as a function of  $k_T$ . The quark accumulation near  $k_T \sim Q_s$ . This is quark saturation.

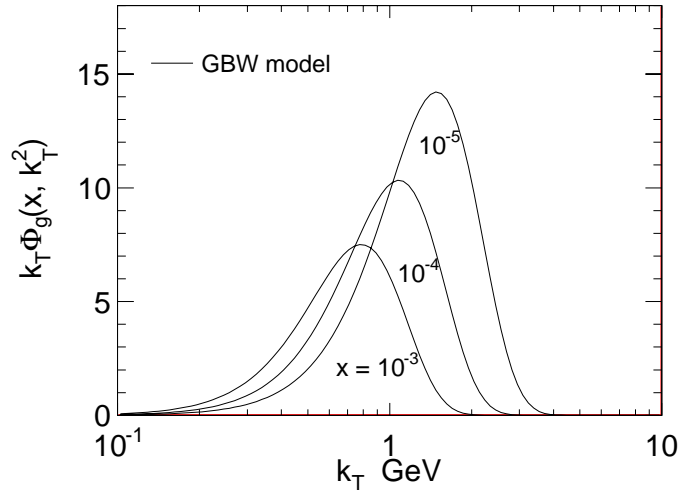


Figure 5: A typical unintegrated gluon distribution simulated by the GBW model [9]. Note that the GBW gluon lacks a  $1/k_T$  tail since the parton evolution is not treated in this model.

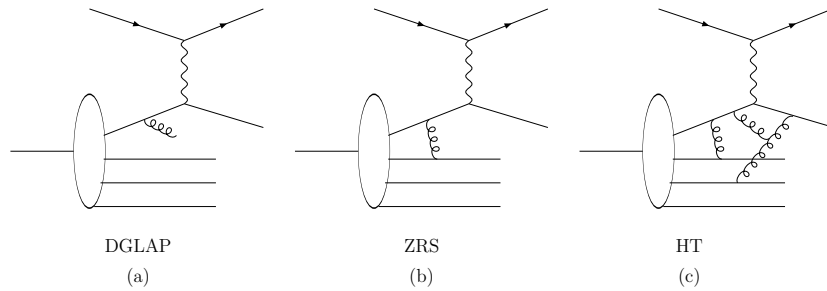


Figure 6: DIS process. (a) The leading twist contributions; (b) A twist-4 corrections; (c) The high twist contributions, which can be isolated by using a naive VMD model.

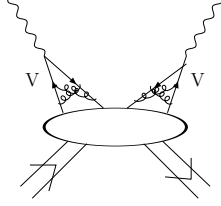


Figure 7: The VMD model.

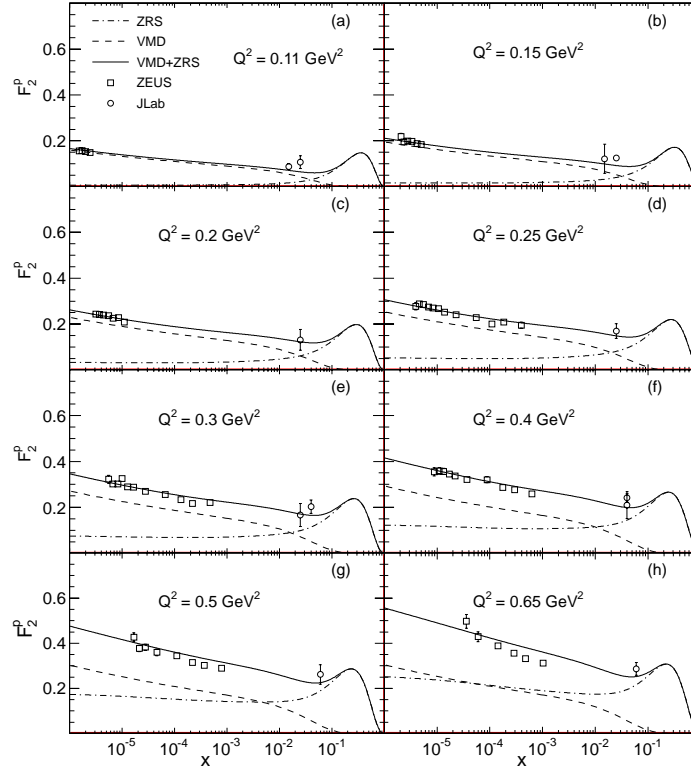


Figure 8: The total proton structure function  $F_2^p(x, Q^2)$  as a function of  $x$  at various  $Q^2$  values ( $< 1 \text{ GeV}^2$ ). The contributions of  $F_2^{\text{hadron}}(x, Q^2)$  and  $F_2^p(x, Q^2)$  are indicated. The data are taken from [13-15]. One can find that a flattish quark distribution hides under measured structure function.

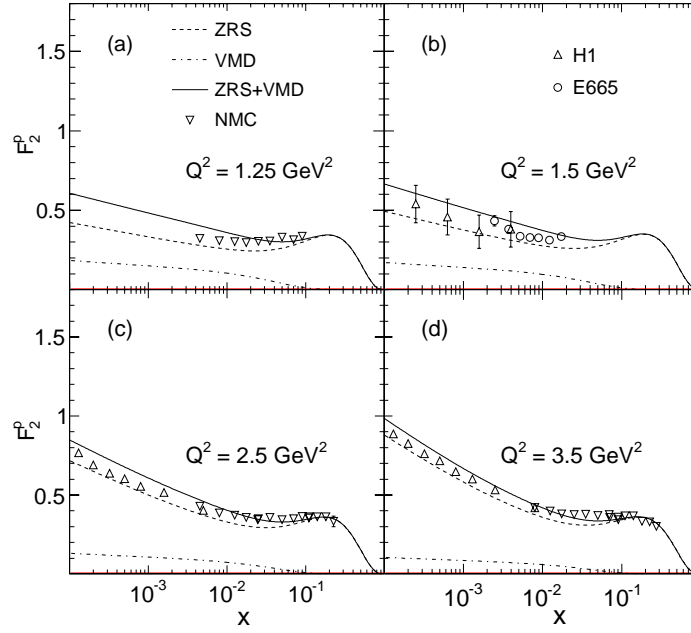


Figure 9: Same as Fig. 8 but for  $Q^2 > 1\text{GeV}^2$

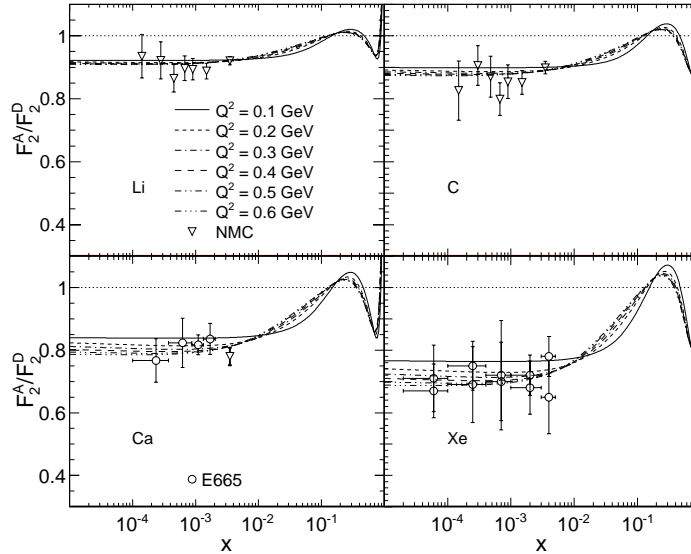


Figure 10: Predicted ratio of  $F_2^A/F_2^p$  for several nuclei at  $Q^2 < 1\text{GeV}^2$  and the comparison with the data [16,17]. The platform origins partly from the quark saturation.

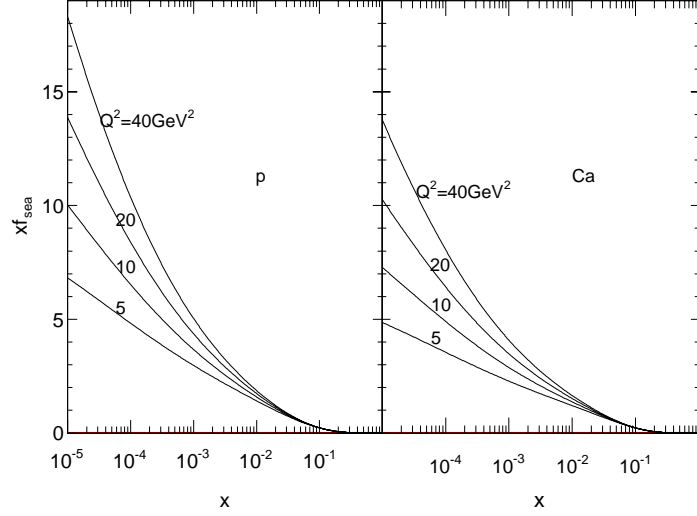


Figure 11: Sea quark distributions in proton and calcium at  $Q^2 = 5 - 40 \text{ GeV}^2$ .

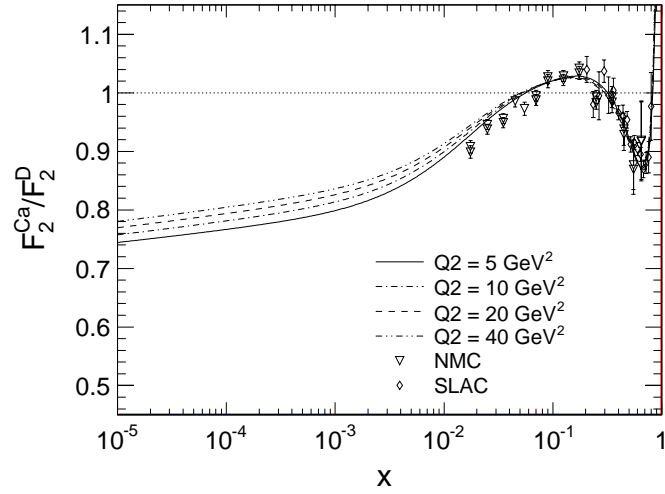


Figure 12: Predicted ratio for  $F_2^{\text{Ca}}/F_2^{\text{p}}$  at  $Q^2 \gg 1 \text{ GeV}^2$ , which presents the different  $Q^2$ - and  $x$ -dependence.



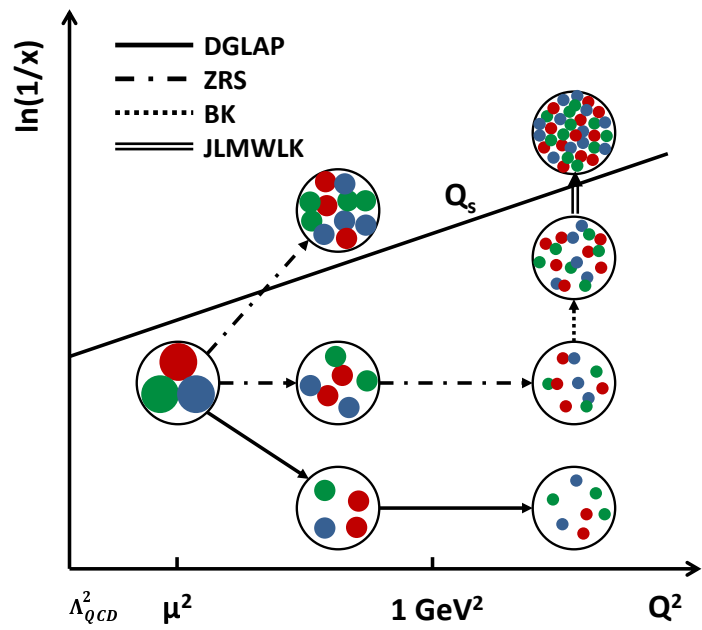


Figure 13: A schematic diagram for illustrating the evolution of parton distributions in different kinematic regions.